Phase-model analysis of coupled neuronal oscillators with multiple connections

Dong-Uk Hwang,[1] Sang-Gui Lee,[2] Seung Kee Han,[1] and Hyungtae Kook[3,4,*]
[1]*Department of Physics, Chungbuk National University, Cheongju 361-763, Korea*
[2]*Department of Physics, Kyungpook National University, Daegu, 702-701, Korea*
[3]*Department of Physics, Kyungwon University, Sungnam 461-701, Korea*
[4]*Asia Pacific Center for Theoretical Physics, POSTECH, Pohang 790-784, Korea*
(Received 26 May 2006; revised manuscript received 26 August 2006; published 22 September 2006)

Synchronization of the coupled neuronal oscillators with multiple connections of different coupling nature is analyzed using the phase-model reduction method. Each coupling connection contributes to the dynamic behavior of the system in a complex nonlinear fashion. In the phase-model scheme, the contribution of the individual connections can be separated in terms of the effective coupling functions associated with each connection and a linear superposition of them provides the total effective coupling of the coupled system. The case of multiple connections with various conduction time delays is also examined, which is shown to be capable of promoting synchronization over an ensemble of spatially distributed neuronal oscillators in an efficient way.

DOI: 10.1103/PhysRevE.74.031911 PACS number(s): 87.19.La, 05.45.Xt, 87.10.+e

I. INTRODUCTION

The brain is a complex dynamical system consisting of an extraordinarily large number of units of neurons with even a larger number of interconnections among them. Synchronous firing of neurons has received much attention in relation to the generation of brain wave rhythms and information processing at various aspects in the neuronal systems [1–3]. Synchronization has also been addressed as an important issue in diverse fields ranging from the physical and biological to social sciences [4,5].

Rhythms in the various frequency ranges are found in many parts of the nervous system, which are considered to be associated with information processing in the brain. The γ (30–80 Hz) and the β (12–30 Hz) rhythms have been observed in the CA1 area of the hippocampus [6,7]. Recently, the underlying mechanism for the stability of these rhythms has been studied with the neuronal oscillator network model for the hippocampal CA1 area [8,9]. These works have shown that the frequency range of the stable rhythms is correlated with the range of the interactions among the neuronal units; the γ rhythms are stable only in the local area, and in the presence of significant conduction time delay in the long-range interaction only the β rhythms remain stable. Especially, it has been pointed out that the role of long-range excitatory connections is essential for β rhythm synchronization. However, the separate contributions of individual connections in multiply connected neuronal oscillators have not been thoroughly understood.

The time-delayed coupling between neuronal oscillators arises naturally from the neurophysiological origins in processes such as synaptic transmission and axonal propagation of the action potentials. The effect of the time delay on the stability of synchronization has been studied extensively in a wide class of neuronal oscillator models including integrate-and-fire neurons [10,11], FitzHugh-Nagumo neurons [12], and Hodgkin-Huxley neurons [13,14].

The phase oscillator model has been introduced for analyzing the dynamics of coupled nonlinear oscillators [15]. The phase description of each oscillator enables us to reduce drastically the complexity of the original system. The most valuable benefit of the reduction might be the feasibility of estimating the effective coupling between oscillators, which is attained via the effective coupling function. The phase-model analysis has been successful especially in analyzing the various synchronization phenomena [13,16–20].

In this paper we study coupled neuronal oscillators that have multiple connections, focusing on the roles of the individual connections in their contribution to the synchronization. As an example, we reexamine the hippocampal CA1 model in which the neuronal oscillator units are connected with multiple connections of different synaptic nature. We exploit the phase-model reduction method to explore the complex nonlinear behavior of the original system; in this scheme, the total effective coupling between oscillators is simply given as a linear superposition of the individual effective coupling arising from each connection. The results from the phase-model analysis are shown to be consistent with direct simulations of the original system. The nonlinear behavior of the coupled system is also presented with the aid of the associated bifurcation diagram. Synchronization over an ensemble of spatially distributed neuronal oscillators is also examined by incorporating different conduction time delays into the multiple connections. It is shown that multiple connections with different time delays can promote synchronization over an oscillator ensemble in an efficient way.

The paper is organized as follows. Section II decribes briefly the phase-model reduction method. A simplified version of the hippocampal CA1 model as an example of the coupled neuronal oscillators with multiple connections is described in Sec. III with some details given separately in the Appendix. Some previous results relevant to the present interests are also included. In Sec. IV, the coupling connections

*Corresponding author. Electronic address: hkook@kyungwon.ac.kr

 ©2006 The American Physical Society

of different natures are considered and the roles of individual connections are analyzed. Section V treats the case of the coupled system which has multiple connections of the various conduction time delays. Finally, a summary and discussions are given in the last section.

II. PHASE-MODEL REDUCTION METHOD

To illustrate the method we consider a system of two identical limit-cycle oscillations of period T coupled with multiple connections:

$$\frac{d\mathbf{X}_{1,2}}{dt} = \mathbf{F}(\mathbf{X}_{1,2}) + \sum_i c_i \mathbf{p}^i(\mathbf{X}_{1,2}, \mathbf{X}_{2,1}), \tag{1}$$

where $\mathbf{X}_j$ is the state vector of the jth oscillator, $\mathbf{F}$ the uncoupled vector field, $\mathbf{p}^i$ the coupling through the ith connection, and c_i the corresponding coupling strength, respectively.

The phase model applies in the limit of weak coupling where the coupling raises only a negligible perturbation to the limit cycle of the uncoupled oscillators [15]. The phase variables ϕ_1 and ϕ_2 can be introduced to parametrize the evolution of the vector $\mathbf{X}_0$ on the limit cycles of the uncoupled oscillators: each phase ϕ satisfies $d\phi(\mathbf{X}_0)/dt = \omega$, where $\omega = 2\pi/T$ is a constant. The definition of the phase can be also extended over the whole state space.

In the presence of a perturbation, as for the case of the coupled oscillators, the phase dynamics is modified as

$$\frac{d\phi_1}{dt} = \omega + \sum_i c_i \Gamma^i(\Delta\phi),$$

$$\frac{d\phi_2}{dt} = \omega + \sum_i c_i \Gamma^i(-\Delta\phi), \tag{2}$$

where the phase difference is denoted as $\Delta\phi \equiv \phi_1 - \phi_2$. The effective coupling function Γ^i associated with $\mathbf{p}^i$ is given as

$$\Gamma^i(\Delta\phi) = \frac{1}{2\pi}\int_0^{2\pi} \mathbf{Z}(\phi) \cdot \mathbf{p}^i(\phi, \Delta\phi) d\phi, \tag{3}$$

where the sensitivity function defined as $\mathbf{Z}(\phi) \equiv \nabla_{\mathbf{X}}\phi|_{\mathbf{X}_0}$ measures the phase-dependent response of the uncoupled oscillator ($\mathbf{X}_0$) to the perturbation.

The interplay between two oscillators is often described by the evolution of the phase difference $\Delta\phi$, which is shown to be determined solely by the antisymmetric part of the effective coupling function: $\Gamma^i_-(\Delta\phi) = \Gamma^i(\Delta\phi) - \Gamma^i(-\Delta\phi)$. That is, the dynamics of $\Delta\phi$ is given as

$$\frac{d\Delta\phi}{dt} = \Gamma^{total}_-(\Delta\phi) = \sum_i c_i \Gamma^i_-(\Delta\phi). \tag{4}$$

The total effective function is just a linear combination of the effective coupling functions associated with each coupling connection. The zeros of Γ^{total}_- are the fixed points of Eq. (4) which correspond to the phase-locked states and their stabilities are determined from the slope of Γ^{total}_- at the corresponding fixed points; negative slope means that the fixed point is a stable state and the nearby $\Delta\phi$ dynamically converges to the fixed point. Positive slope means that the fixed point is an unstable state and the nearby $\Delta\phi$ dynamically diverges away from the fixed point. The amplitude of Γ^{total}_- determines the convergence (divergence) rate at the fixed point.

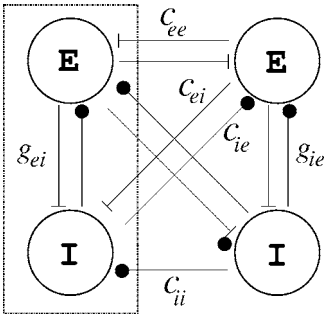

FIG. 1. Schematic diagram of the coupled neuronal oscillator model. Each oscillator unit, denoted by a box, consists of one excitatory neuron (E cell) and one inhibitory neuron (I cell). The synaptic connections are denoted using g's for the intraco lumnar connections and c's for the intercolumnar connections. The subscripts of the variables are given following the "from-to" rule; c_{ei} refers to the connection from the E cell to the I cell, for instance.

III. COUPLED NEURONAL OSCILLATORS WITH MULTIPLE CONNECTIONS

In this paper as an example of the coupled neuronal oscillators with multiple connections we use the model for the hippocampal CA1 area of the brain that has been adopted to explore the dynamic stability of the gamma and the beta rhythms [8,9]. Here the model is more simplified to focus on the exploration of the multiple connections between coupled neuronal oscillators.

A schematic diagram for the columnar structure of the CA1 model is presented in Fig. 1. Each column consists of one excitatory neuron (E cell) and one inhibitory neuron (I cell). The intracolumnar connections bind two cells into an oscillator. That is, each column is regarded as an oscillator unit. The intercolumnar connections then provide coupling between two neuronal oscillators. The intercolumnar couplings can be of long range, and such an effect is considered in the model by incorporating the conduction time delay as is shown in the later section.

The membrane voltage dynamics of the E cell is described by the conductance-based neuronal model of Hodgkin-Huxley type:

$$C\frac{dV}{dt} = -g_l(V - E_l) - g_{\mathrm{Na}} m^3 h (V - E_{\mathrm{Na}}) - g_{\mathrm{K}} n^4 (V - E_{\mathrm{K}}) - g_{\mathrm{AHP}} w (V - E_{\mathrm{K}}) - I^{syn}_e + I^{appl}_e. \tag{5}$$

The equation for the I cell is identical except that there is no after-hyperpolarization (AHP) current—i.e., $g_{\mathrm{AHP}} = 0$; the AHP current arises from a type of ion channels with the nature of slow K conductance. We will use the subscripts e

and i to distinguish symbols for the excitatory and inhibitory cells, respectively, whenever it is needed. The variables m, h, n, and w describe the gating dynamics for the ion flow at each ion channel, and the governing equations are summarized in the Appendix.

The synaptic currents can be grouped into two classes: intracolumnar and intercolumnar synaptic currents—that is, $I_e^{syn}=I_e^{intra}+I_e^{inter}$ and $I_i^{syn}=I_i^{intra}+I_i^{inter}$. Each term is given as

$$I_e^{intra} = g_{ie}s_i(t)(V-E_{inh}),$$

$$I_e^{inter} = c_{ee}\bar{s}_e(t)(V-E_{ex}) + c_{ie}\bar{s}_i(t)(V-E_{inh}),$$

$$I_i^{intra} = g_{ei}s_e(t)(V-E_{ex}),$$

$$I_i^{inter} = c_{ei}\bar{s}_e(t)(V-E_{ex}) + c_{ii}\bar{s}_i(t)(V-E_{inh}), \tag{6}$$

where the g's are the conductances of the intracolumnar synaptic connections, while the c's are the conductances of the intercolumnar synaptic connections. In all simulations, we set $g_{ie}=1.0$, and $g_{ei}=0.3$. The variables $s(t)$ and $\bar{s}(t)$ describe the temporal variation of the synaptic currents from the intracolumnar and the intercolumnar presynaptic cells, respectively. Their governing equations are given in the Appendix. Note that the barred and unbarred variables satisfy the same form of the equations. The parameters E_{ex} and E_{inh} are the postsynaptic reversal potentials for the excitatory and inhibitory synapses, respectively. All the parameters are set in accordance with the standard experimental setup and are also presented in the Appendix.

From typical simulations for the single column oscillator, we find that either the increase of I_e^{appl} or the decrease of g_{AHP} results in the higher firing rate of the E cell; these parameters modulate the excitability of the E cell in the opposite directions [9]. It has been observed that various states of phase-locked firings between the E cell and I cell arise in which the ratio of the firing rates of the cells is determined depending on the magnitudes of the two parameters I_e^{appl} and g_{AHP} for a fixed value of I_i^{appl}. For example, when $g_{\mathrm{AHP}}=0$, $I_e^{appl}=7.9$, and $I_i^{appl}=0.5$, the column oscillator is 1:1 locked; the E cell and I cell fire synchronously. Meanwhile, when the excitability of the E cell is suppressed by increasing g_{AHP}—for example, when $g_{\mathrm{AHP}}=1$—the column oscillator becomes 1:2 locked; the I cell fires twice during one firing period of the E cell.

In the hippocampal CA1 model, the synchronized firing of an ensemble of columnar oscillators that are all 1:1 phase-locked is responsible for the generation of the γ rhythm, while the synchronization of the 1:2 phase-locked oscillators is responsible for the generation of the β rhythm [9]. The existence of the 1:2 locking at each oscillator alone is, however, insufficient for the generation of the β rhythm. That is, the columns in the β oscillation should be synchronized and the synchronization should be a stable state as well. Previous works have shown that the sufficient condition is fulfilled with the aid of the long-range intercolumnar excitatory synaptic connections [8,9].

All the simulations shown in this paper have been done in the parameter range where each column oscillator is in the 1:2 locking state. Specifically, we set $g_{\mathrm{AHP}}=1$, $I_e^{appl}=7.9$, and $I_i^{appl}=0.5$. The coupled neuronal oscillator system is shown to have various stationary states of the phase-locked relation. We then focus on analyzing the effect of the multiple synaptic connections on the stability and the bifurcation of those stationary states.

IV. MUTIPLE CONNECTIONS OF DIFFERENT COUPLING NATURE

The limit cycle $\mathbf{X}_0$ and the sensitivity function $\mathbf{Z}(\phi)$ are numerically calculated. The normalized effective coupling functions for each synaptic connection are obtained from the following integrations [14,15]:

$$\Gamma^{ee}(\Delta\phi) = \frac{1}{2\pi}\int_0^{2\pi} Z_e(\phi)\bar{s}_e(\Delta\phi)V_e(\phi)d\phi,$$

$$\Gamma^{ii}(\Delta\phi) = \frac{1}{2\pi}\int_0^{2\pi} Z_i(\phi)\bar{s}_i(\Delta\phi)[V_i(\phi)+80]d\phi,$$

$$\Gamma^{ie}(\Delta\phi) = \frac{1}{2\pi}\int_0^{2\pi} Z_e(\phi)\bar{s}_i(\Delta\phi)[V_e(\phi)+80]d\phi,$$

$$\Gamma^{ei}(\Delta\phi) = \frac{1}{2\pi}\int_0^{2\pi} Z_i(\phi)\bar{s}_e(\Delta\phi)V_i(\phi)d\phi. \tag{7}$$

Here the functions $Z_e(\phi)$ and $Z_i(\phi)$ denote the V_e and V_i components of $\mathbf{Z}(\phi)$, respectively.

The antisymmetric part of the normalized effective coupling function for each synaptic connection is shown in Figs. 2(a)–2(d). In each plot the fixed points are denoted using squares for the stable points and circles for the unstable points. The temporal evolution of $\Delta\phi$ starting from different initial conditions is also shown in the corresponding right panels in Figs. 2(e)–2(h). The behavior of the effective coupling function and the evolution of $\Delta\phi$ are shown for each connection separately. The details of the analysis are summarized below for each synaptic connection.

(i) *E-E connection*. The function Γ_-^{ee} in Fig. 2(a) has roots at $\Delta\phi=0$ with a negative slope and at $\Delta\phi=\pi$ with a positive slope; the two states with $\Delta\phi=\pm\pi$ are equivalent since the effective coupling functions are 2π periodic by definition. The fixed point at $\Delta\phi=0$ is a unique stable state in this case. Therefore, the phase-model analysis predicts that the phase difference of any initial values except $\Delta\phi=\pi$ would eventually converge to $\Delta\phi=0$. This result can be verified by directly integrating the original equation (5) with various initial values of $\Delta\phi$. These simulation results are also shown aside in Fig. 2(e). The analysis together with the numerical simulation, therefore, shows that the E-E connection has the role of stabilizing the in-phase synchronization of the coupled oscillators. Notice that the slope of Γ_-^{ee} at $\Delta\phi=\pi$ is very small, which implies a weakness of the unstable state; $\Delta\phi$ starting near $\Delta\phi=\pi$ escapes from the fixed point very slowly.

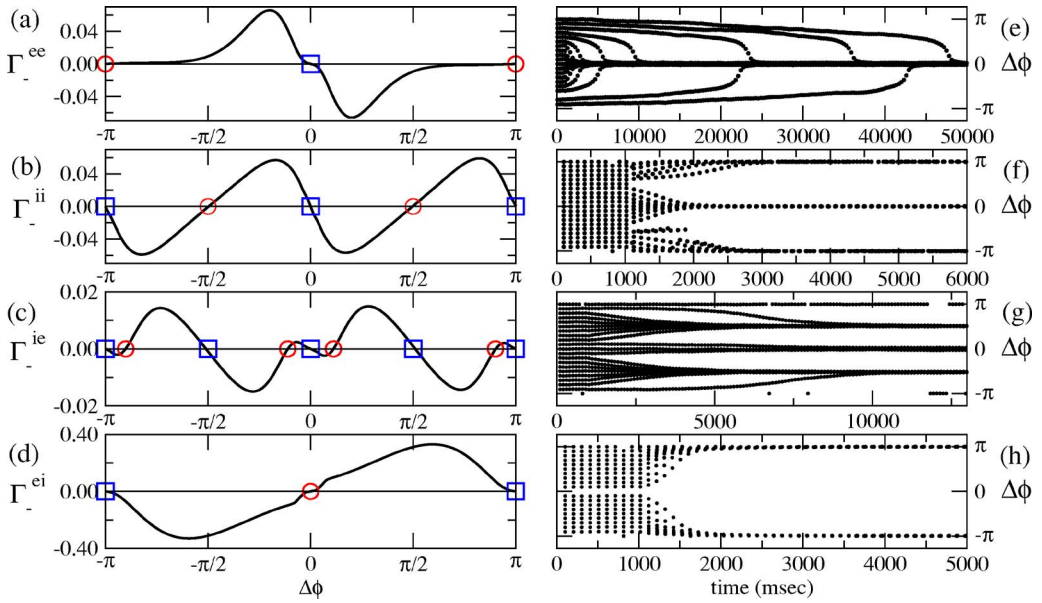

FIG. 2. (Color online) The antisymmetric part of the effective coupling function associated with each connection (a)–(d). The circles denote the unstable fixed points, and the squares denote the stable fixed points. The time courses of the phase difference are plotted starting at various initial conditions for each connection (e)–(h). An initial period of 1000 msec before turning on the connection is given for every plot for better tracing the time course. The horizontal axes are rescaled according to the convergence rates. The (coupling) connection strength is set as $c=0.01$ for all simulations.

Recall that the E cell and I cell in the column are 1:2 locked; every other firing of the I cell inhibits the firing of the E cell, which makes the firing period T of the E cell twice that of the I cell. The antiphase state corresponds to alternating firings between the intercolumnar E cells. In this situation a competition exists for firing an E cell between the inhibition from the intracolumnar I cell and excitation through the intercolumnar E-E connection. The instability of the antiphase state implies that the inhibition from the I cell is yet strong enough to make the excitation from the E cell ineffective. The small values of Γ_{delay-} near $\Delta\phi=\pi$ in Fig. 2(a) also indicate that this inhibition is dominant in the wide range of $\Delta\phi$ near $\Delta\phi=\pi$.

(ii) *I-I connection*. The function Γ_-^{ii} has two stable fixed points at $\Delta\phi=0$, π and two unstable fixed points at $\Delta\phi=\pm\pi/2$ as shown in Fig. 2(b). The unstable states form the boundaries for the attraction basins of the stable states as can be seen from Fig. 2(f). The I-I connection stabilizes two states which are the in-phase and the antiphase synchronization, respectively. This bistability can be surpassed with the dominance of the in-phase synchronization by incorporating a strong E-E coupling connection, which has been proposed as an underlying mechanism for the transition between the γ rhythm and β rhythm observed in the hippocampal CA1 area of the brain [8,9]. Notice that the I-I connection gives rise to an indirect interaction between E cells via the intracolumnar connections.

(iii) *I-E connection*. The function Γ_-^{ie} has four stable fixed points at $\Delta\phi=0$, $\pm\pi/2$, and π and four unstable fixed points pairwisely located near the stable fixed points at $\Delta\phi=0$ and π as shown in Fig. 2(c). The unstable states form the boundaries for the attraction basins as seen from Fig. 2(g). The I-E connection stabilizes three states: the in-phase, the antiphase, and the out-of-phase states, respectively. The in-phase synchronization is stable even though its attraction basin is only small. The stable states at $\Delta\phi=\pm\pi/2$ are the most dominant in that their attraction basins are the largest. Notice that the structure of Γ_-^{ie} is almost exactly reversed compared to that of Γ_-^{ii} except for the existence of small attraction basins at $\Delta\phi=0$ and π. Similar to the I-I connection, the I-E connnection also provides an indirect interaction between the E cells. In this case, however, the path is less indirect in that the I cell is connected directly to the intercolumnar E cell, which might be the origin of the reversed structures of the effective coupling functions.

(iv) *E-I connection*. The function Γ_-^{ei} roughly has the structure reversed from that of Γ_-^{ee} as shown in Figs. 2(d) and 2(h). The role of the E-I connection is stabilizing the antiphase state and preventing the in-phase state, which implies that the indirect interaction between the E cells through the E-I connection in cooperation with the intracolumnar I-E connection destabilizes the in-phase synchronization.

Now, in the presence of multiple connections, the total effective coupling function is given as a superposition of all the constituent effective coupling functions, Eq. (7), multiplied by the corresponding synaptic coupling strengths:

$$\Gamma^{total} = c_{ee}\Gamma^{ee} + c_{ii}\Gamma^{ii} + c_{ie}\Gamma^{ie} + c_{ei}\Gamma^{ei}. \tag{8}$$

Notice that the original system, Eq. (1), is highly nonlinear, especially in those perturbative coupling connections. Meanwhile, Eq. (8) shows that the total effect of the multiple connections is given as a nice linear superposition of the contributions from the individual connections. This is the very advantage of using the phase-model reduction method.

The nonlinear bahavior of the system can now be analyzed rather straightforwardly by examining the function

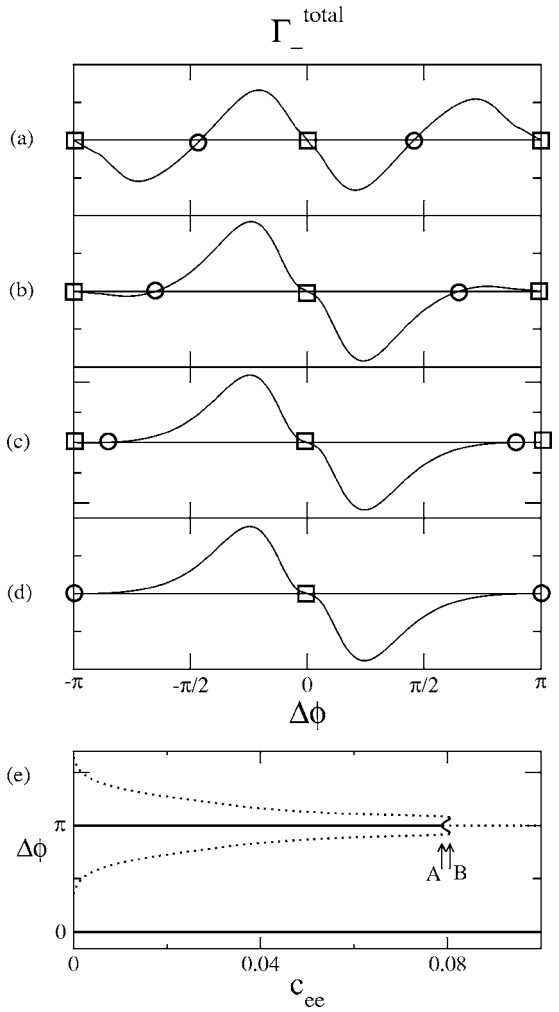

FIG. 3. The antisymmetric part of the total effective coupling function. The nonlinear evolution of Γ_{-}^{total} is shown as c_{ee} is increased: (a) $c_{ee}=0.001$, (b) $c_{ee}=0.01$, (c) $c_{ee}=0.05$, and (d) $c_{ee}=0.1$. The other parameters remain fixed as $c_{ii}=0.002$, $c_{ei}=0$, and $c_{ie}=0.005$. The circles denote the unstable fixed points, and the squares denote the stable fixed points. The bifurcation structure of the antiphase state is shown in detail in the panel (e). *A* denotes the pitchfork bifurcation point at $c_{ee}\sim 0.0788$, and *B* denotes the saddle-node bifurcaton point at $c_{ee}\sim 0.0807$. The traces of the stable states and the unstable states are denoted with the solid lines and the dotted lines, respectively. The in-phase state at $\Delta\phi=0$ remains stable in this range of c_{ee}.

Γ_{-}^{total}. To be specific, we set $c_{ii}=0.002$, $c_{ei}=0$, and $c_{ie}=0.005$ and vary c_{ee} from 0.001 to 0.1. The total effective coupling functions for each case are shown in Fig. 3(a)–3(d). For small values of c_{ee} the in-phase and antiphase states are stable fixed points and there also exist a pair of the out-of-phase states which are unstable. As c_{ee} is increased, however, those unstable out-of-phase states approach the antiphase state. Eventually, as shown in Fig. 3(d), the out-of-phase states disappear and the stable antiphase state becomes unstable.

The details of the above bifurcation scenario are examined and presented in Fig. 3(e). As one can see in the figure, as c_{ee} is increased, the stable antiphase state undergoes the supercritical pitchfork bifurcation at $c_{ee}\sim 0.0788$ (denoted by *A* in the figure). At this point the antiphase state becomes unstable and a pair of the stable out-of-phase states are born. These stable out-of-phase states collide in pair with unstable out-of-phase states that are shown in Figs. 3(a)–3(c) and disappear at $c_{ee}\sim 0.0807$ through the saddle-node bifurcation (denoted by *B*). Notice that the in-phase state at $\Delta\phi=0$ remains stable in this range of c_{ee}.

V. MULTIPLE CONNECTIONS WITH TIME DELAYS

The analysis of the preceding section shows how to locate the parameter regime of the stable synchronization. However, the existence of the stable synchronization, even together with its uniqueness, may be yet insufficient in establishing itself in a practical sense. Then, the convergence rate to the synchronization becomes important. For instance, as we have already seen such a hint from Fig. 3(d), the convergence to the existing synchronized state can take a long time. Especially, this slow convergence can be a crucial problem in establishing synchronization over an ensemble of spatially distributed neuronal oscillators. In this section we will show that the multiple connections with different conduction time delay among neuronal oscillators can promote synchonization over an oscillator ensemble in an efficient way.

In our present model the above-mentioned slow convergence is the most problematic for the E-E connection case, which is noticeable from the behavior of the effective coupling functions as shown in Fig. 2; the shape of the effective coupling functions is attributed to the specific nonlinear feature of the limit cycle in consideration. Therefore, we here consider only the effect of the intercolumnar E-E connections and shut off all the other intercolumnar connections. The superscript in Γ^{ee} will be omitted for simplicity. The intercolumnar synaptic current to the E cell of Eq. (6) is then modified as

$$I_e^{inter}=\sum_j c_{ee}^j \bar{s}_e(t-\tau_j)V, \tag{9}$$

where c_{ee}^j is the jth E-E connection with the conduction time delay τ_j.

The evolution of the phase difference $\Delta\phi$, Eq. (4), is also modified as [14]

$$\frac{d\Delta\phi}{dt}=\Gamma_{delay-}^{total}(\Delta\phi)=\sum_j c_{ee}^j \Gamma^j{}_{delay-}(\Delta\phi)$$
$$=\sum_j c_{ee}^j[\Gamma(\Delta\phi+\delta_j)-\Gamma(-\Delta\phi+\delta_j)], \tag{10}$$

where $\delta_j=2\pi\tau_j/T$ and $T=50.9$ msec. Similar to Eq. (4), the total effective coupling function is given as a linear superposition of the effective coupling functions with different time delays [9].

The effect of the time delay can be understood in an intuitive way using graphs. First, consider the case of no time delay as a reference. The effective coupling function $\Gamma(\Delta\phi)$ is plotted using a solid line in Fig. 4(a). The antisymmetric part of $\Gamma(\Delta\phi)$ is obtained first by reflecting it with repect to

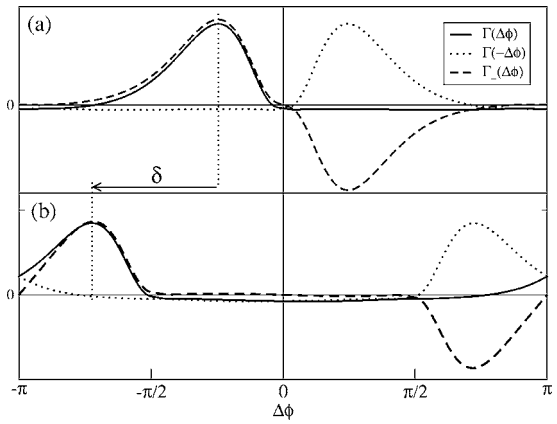

FIG. 4. The effect of time delay on the effective coupling functions. The case of no time delay is shown for reference in (a) and the case of time delay $\tau=13$ msec is shown below in (b). The original effective coupling function, its reflected graph, and its antisymmetric part are plotted together in each panel using different line types: the solid, the dotted, and the dashed lines, respectively.

$\Delta\phi=0$ to get $\Gamma(-\Delta\phi)$ and substracting this from $\Gamma(\Delta\phi)$. The graphs for $\Gamma(-\Delta\phi)$ and $\Gamma_{-}(\Delta\phi)$ are plotted using a dotted line and a dashed line, respectively. From the construction scheme, one can notice that $\Delta\phi=0$ and $\Delta\phi=\pi$ are always zeros of $\Gamma_{-}(\Delta\phi)$ which correspond to the fixed points of Eq. (10). The stability of each fixed point is determined again from the slope of $\Gamma_{-}(\Delta\phi)$, which is just the doubled slope of $\Gamma(\Delta\phi)$ from the construction scheme.

Now, let us consider the case of time delay and take $\tau=13$ msec specifically. This time delay leads to a phase shift of the effective coupling function by the amount of $\delta=2\pi\tau/T$. The result is the left-shifted graph of $\Gamma(\Delta\phi+\delta)$ as plotted with a solid line in Fig. 4(b). Its antisymmetric part $\Gamma(\Delta\phi+\delta)-\Gamma(-\Delta\phi+\delta)$ is constructed in the same way as above, and the corresponding graphs are plotted using the same line types. Again, the stability of the fixed points is determined from the doubled slope of $\Gamma(\Delta\phi+\delta)$ at each fixed point. The in-phase state at $\Delta\phi=0$ in this specific case turns out to be stable since the minimum of $\Gamma(\Delta\phi+\delta)$, yet lies in the positive side of $\Delta\phi$, and thus the slope $\Gamma(\Delta\phi+\delta)$ at $\Delta\phi=0$ is negative. Notice that the peaks of $\Gamma_{-}(\Delta\phi)$ are shifted by the amount of δ in both directions away from $\Delta\phi=0$.

In the presence of multiple connections, the role of each synaptic connection can be understood in the similar procedure as in the preceding section. To understand how the multiple connections work, it suffices to examine the simplest case. That is, we will consider the case of two connections with time delay $\tau_1=0.5$ msec and $\tau_2=13$ msec. The effective coupling functions for the individual connections and in the presence of the both connections are shown in Fig. 5 together with the time evolution of the phase difference for each case.

From Fig. 5(a), in comparison with Fig. 2(a), it is seen that the effective coupling function for the time delay $\tau_1=0.5$ msec is almost same as for the case of no time delay. The function Γ_{delay-} has basically the same structure: two fixed points at $\Delta\phi=0$ and π. Only the maximum and minimum peaks shift slightly away from $\Delta\phi=0$. The fixed point at $\Delta\phi=0$ corresponds to the stable in-phase state. Since the magnitude of Γ_{delay-} determines the convergence rate, one can notice that the initial values near $\Delta\phi=0$ converge rapidly toward the in-phase state, as can be confirmed from Fig. 5(d). The other fixed point at $\Delta\phi=\pi$ corresponds to the antiphase state. The antiphase state is unstable since Γ_{delay-} has the positive slope. Therefore, the nearby initial $\Delta\phi$'s diverge away. That is, any initial values of $\Delta\phi$ except π fall in the attraction basin of the in-phase state and all are attracted to $\Delta\phi=0$ asymptotically in time. However, as noticed from the small magnitude of Γ_{delay-}, the divergence rate is very small and the attraction is very slow as can be confirmed from Fig. 5(d). Notice the elongated time scale of the convergence in the figure.

When the time delay is $\tau_2=13$ msec, comparable to the period T, the shift of the peaks become even larger as shown

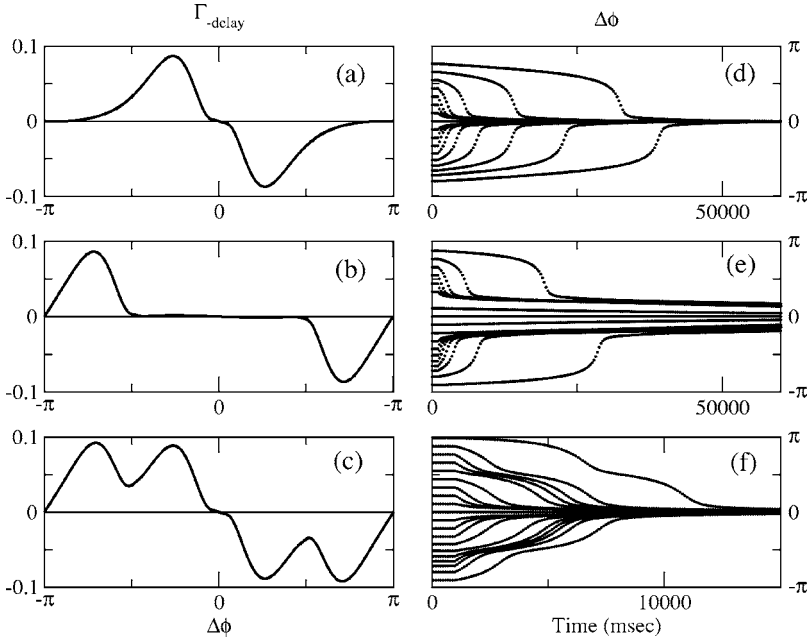

FIG. 5. The antisymmetric part of the effective coupling functions in the presence of the conduction time delay. The time courses of the phase difference are plotted together in the right panels starting at various initial conditions. The plots are when a single connection with the time delay $\tau=0.5$ msec exists (a), (d), when a single connection with the time delay $\tau=13$ msec exists (b), (e), and when the multiple connections including the both exist together (c), (f).

in Fig. 5(b). The stability of the fixed points remains the same as for the case of $\tau_1=0.5$ msec. However, the more important change occurs in the speed of the $\Delta\phi$ dynamics. The convergence to the in-phase state becomes very slow near $\Delta\phi=0$; notice the time scale of the convergence in Fig. 5(e). Meanwhile, the initial values near the antiphase state diverge away very rapidly. That is, the role of the time delay of $\tau_2=13$ msec is a strong destabilization of the antiphase state. As one can see from Fig. 2, the E-E connection is the only source for the instability of the antiphase state. However, the E-E connection alone is ineffective since the divergence rate from the antiphase state is extremely small, as argued with Fig. 2(a) in the preceding section. Here, one can realize that a sufficient amount of the time delay provides an effective way in destabilizing the antiphase state.

When the connection is multiple with two different time delays together, the corresponding function Γ^{total}_{delay-} is just a superposition of the effective coupling functions for individual connections, as shown in Fig. 5(c). The stability of the fixed points still remains the same. However, the dynamics of $\Delta\phi$ now manifests both features of the individual connections: the rapid divergence from the antiphase state and the rapid convergence to the in-phase state. Consequently, over a wider range of initial values of $\Delta\phi$ the in-phase synchronization can be established rather rapidly; notice the drastic change in the time scale of the convergence in Fig. 5(f).

One can straightforwardly extend our analysis to the case of the multiple connections with various time delays among neuronal oscillators. In this case each connection of different time delay plays the role of a relay midway to pushing $\Delta\phi$ from the antiphase toward the in-phase state. Therefore, the multiple connections with different time delays can promote synchonization over an oscillator ensemble in an efficient way.

VI. SUMMARY AND DISCUSSION

Synchronization of the coupled neuronal oscillators with multiple connections is analyzed, focusing on the roles of the individual connections in their contribution to the synchronization. The dynamics of the phase difference between the oscillators are well described in the scheme of phase-model reduction, which is determined solely from the total effective coupling function. The total effective coupling function is given just as a linear superposition of the individual effective coupling functions associated with each connection. The fixed points corresponding to the various phase-locked states are identified. The shape of the effective coupling function determines the existence and the stability of those fixed point. The convergence and divergence rates near the fixed point are also determined from the amplitude of the effective coupling function. The bifurcation analysis clarifies how the coupling nature of the system changes in a nonlinear fashion and how the stable antiphase state loses its stability and the in-phase state becomes prevalent, which provides an intuitive understanding of the transition from the γ rhythm to the β rhythm observed in the brain.

The conduction time delay in the coupling connection induces the amplitude peaks of the effective coupling function to shift toward the antiphase state. When the amount of the time delay is comparable to the period T of the oscillation, this implies that the divergence rate from the antiphase state can be enhanced significantly. In the presence of multiple connections with different time delays, each connection plays a role of a relay midway to pushing $\Delta\phi$ from the antiphase toward the in-phase state. Therefore, the multiple connections with different time delay can promote synchonization over an oscillator ensemble in an efficient way.

ACKNOWLEDGMENTS

This research was supported by Grant No. M103KV01001103K2201 01130 from the BRC of the 21st CFR Program funded by the MOST, Korea and the SBD of NCRC program at POSTECH. H.K. acknowledges partial support from the Korea Research Center for Theoretical Physics and Chemistry. S.-G.L. acknowledges partial support from the Brain Korea 21 (BK21) project.

APPENDIX: HIPPOCAMPAL CA1 MODEL

In addition to Eq. (5), the full equation for the coupled oscillator model includes the equations for the gating variables. The gating variables m, h, n, and w satisfy the following equations, respectively:

$$\frac{dm}{dt}=\frac{0.32(54+V)}{1-e^{-(V+54)/4}}(1-m)-\frac{0.28(V+27)}{e^{(V+27)/5}-1}m,$$

$$\frac{dh}{dt}=0.128e^{-(50+V)/18}(1-h)-\frac{4}{1+e^{-(V+27)/5}}h,$$

$$\frac{dn}{dt}=\frac{0.032(V+52)}{1-e^{-(V+52)/5}}(1-n)-0.5e^{-(57+V)/40}n,$$

$$\frac{dw}{dt}=\frac{w_\infty(V)-w}{\tau_w(V)}, \tag{A1}$$

where

$$w_\infty(V)=1/(1+e^{-(V+35)/10}),$$

$$\tau_w(V)=400/(3.3e^{(V+35)/20}+e^{-(V+35)/20}). \tag{A2}$$

The temporal variation of the synaptic currents, depicted with the variables $s(t)$ and $\bar{s}(t)$, is modeled as the so-called α-function type. $s_e(t)$ and $s_i(t)$ satisfy the following equations, respectively (note that the barred variables for the intercolumnar synapses satisfy the same form of the equations as for the unbarred variables):

$$\frac{ds_e}{dt}=5\left(1+\tanh\frac{V}{4}\right)(1-s_e)-\frac{s_e}{2},$$

$$\frac{ds_i}{dt}=2\left(1+\tanh\frac{V}{4}\right)(1-s_i)-\frac{s_i}{15}. \tag{A3}$$

All parameters of the equations are set in accordance with the standard experimental conditions. The capacitance is set to $C=1\ \mu\mathrm{F/cm^2}$. The g's are the ion channel conductances in $\mathrm{mmho/cm^2}$, and the E's are the reversal potentials in mV for the corresponding ions and synapses: $g_l=0.1$, $g_{\mathrm{Na}}=100$, $g_{\mathrm{K}}=80$, $g_{\mathrm{AHP}}=1$, $E_l=-67$, $E_{\mathrm{Na}}=50$, $E_{\mathrm{K}}=-100$, $E_{ex}=0$, and $E_{inh}=-80$. The applied dc currents are set to $I_e^{appl}=7.9\ \mu\mathrm{A/cm^2}$ for the excitatory neuron and to $I_i^{appl}=0.5\ \mu\mathrm{A/cm^2}$ for the inhibitory neuron.

[1] C. M. Gray, P. König, A. K. Engle, and W. Singer, Nature (London) **338**, 334 (1989).

[2] R. Eckhorn, R. Bause, W. Jordan, M. Brosch, W. Kruse, M. Munk, and H. J. Reitboeck, Biol. Cybern. **60**, 121 (1989).

[3] C. von der Masburg and C. Schneiger, Biol. Cybern. **54**, 29 (1986).

[4] A. Pikovsky, M. Rosenblum, and J. Kurths, *Synchronization: A Universal Concept in Nonlinear Sciences* (Cambridge University Press, Cambridge, England, 2001); S. Boccaletti, J. Kurths, G. Osipov, D. L. Valladares, and C. S. Zhou, Phys. Rep. **366**, 1 (2002).

[5] M. G. Rosenblum, A. S. Pikovsky, and J. Kurths, Phys. Rev. Lett. **76**, 1804 (1996); A. Pikovsky *et al.*, Physica D **104**, 219 (1997).

[6] M. A. Whittington, I. M. Stanford, S. B. Colling, J. G. R. Jefferys, and R. D. Traub, J. Physiol. (London) **502**, 591 (1997).

[7] M. A. Whittington, R. D. Traub, H. J. Faulkner, I. M. Stanford, and J. G. R. Jeffereys, Proc. Natl. Acad. Sci. U.S.A. **94**, 12198 (1997).

[8] N. Kopell, G. B. Ermetrour, M. A. Whittington, and R. D. Traub, Proc. Natl. Acad. Sci. U.S.A. **97**, 1867 (2000).

[9] S.-G. Lee, D.-U. Hwang, S. K. Han, and H. Kook, J. Korean Phys. Soc. **44**, 577 (2004).

[10] S. Coombes and G. J. Lord, Phys. Rev. E **56**, 5809 (1997).

[11] U. Ernst, K. Pawelzik, and T. Geisel, Phys. Rev. E **57**, 2150 (1998).

[12] G. Renversez, Physica D **114**, 147 (1998).

[13] D. Hansel, G. Mato, and C. Meunier, Europhys. Lett. **23**, 367 (1993).

[14] S. Kim, H. Kook, S. G. Lee, and M-H. Park, Int. J. Bifurcation Chaos Appl. Sci. Eng. **8**, 731 (1998).

[15] Y. Kuramoto, *Chemical Oscillations, Waves, and Turbulence* (Springer-Verlag, New York, 1984).

[16] S. K. Han, C. Kurrer, and Y. Kuramoto, Phys. Rev. Lett. **75**, 3190 (1995).

[17] D. Postnov, S. K. Han, and H. Kook, Phys. Rev. E **60**, 2799 (1999).

[18] S. H. Park, S. Kim, H.-B. Pyo, and S. Lee, Phys. Rev. E **60**, 2177 (1999).

[19] O. V. Sosnovtseva, D. E. Postnov, A. M. Nekrasov, E. Mosekilde, and N. H. Holstein-Rathlou, Phys. Rev. E **66**, 036224 (2002).

[20] D. E. Postnov, O. V. Sosnovtseva, S. Y. Malova, and E. Mosekilde, Phys. Rev. E **67**, 016215 (2003).